



An Investigation Into the Grain Structure of Impact Ice

*Rebekah G. Douglass
Pennsylvania State University, State College, Pennsylvania*

*Andrew H. Work, Jr.
Ohio Aerospace Institute, Brook Park, Ohio*

*Richard E. Kreeger
Glenn Research Center, Cleveland, Ohio*

*Ernestina Schirmer
Purdue University, West Lafayette, Indiana*

NASA STI Program . . . in Profile

Since its founding, NASA has been dedicated to the advancement of aeronautics and space science. The NASA Scientific and Technical Information (STI) Program plays a key part in helping NASA maintain this important role.

The NASA STI Program operates under the auspices of the Agency Chief Information Officer. It collects, organizes, provides for archiving, and disseminates NASA's STI. The NASA STI Program provides access to the NASA Technical Report Server—Registered (NTRS Reg) and NASA Technical Report Server—Public (NTRS) thus providing one of the largest collections of aeronautical and space science STI in the world. Results are published in both non-NASA channels and by NASA in the NASA STI Report Series, which includes the following report types:

- **TECHNICAL PUBLICATION.** Reports of completed research or a major significant phase of research that present the results of NASA programs and include extensive data or theoretical analysis. Includes compilations of significant scientific and technical data and information deemed to be of continuing reference value. NASA counter-part of peer-reviewed formal professional papers, but has less stringent limitations on manuscript length and extent of graphic presentations.
- **TECHNICAL MEMORANDUM.** Scientific and technical findings that are preliminary or of specialized interest, e.g., “quick-release” reports, working papers, and bibliographies that contain minimal annotation. Does not contain extensive analysis.
- **CONTRACTOR REPORT.** Scientific and technical findings by NASA-sponsored contractors and grantees.
- **CONFERENCE PUBLICATION.** Collected papers from scientific and technical conferences, symposia, seminars, or other meetings sponsored or co-sponsored by NASA.
- **SPECIAL PUBLICATION.** Scientific, technical, or historical information from NASA programs, projects, and missions, often concerned with subjects having substantial public interest.
- **TECHNICAL TRANSLATION.** English-language translations of foreign scientific and technical material pertinent to NASA's mission.

For more information about the NASA STI program, see the following:

- Access the NASA STI program home page at <http://www.sti.nasa.gov>
- E-mail your question to help@sti.nasa.gov
- Fax your question to the NASA STI Information Desk at 757-864-6500
- Telephone the NASA STI Information Desk at 757-864-9658
- Write to:
NASA STI Program
Mail Stop 148
NASA Langley Research Center
Hampton, VA 23681-2199



An Investigation Into the Grain Structure of Impact Ice

*Rebekah G. Douglass
Pennsylvania State University, State College, Pennsylvania*

*Andrew H. Work, Jr.
Ohio Aerospace Institute, Brook Park, Ohio*

*Richard E. Kreeger
Glenn Research Center, Cleveland, Ohio*

*Ernestina Schirmer
Purdue University, West Lafayette, Indiana*

National Aeronautics and
Space Administration

Glenn Research Center
Cleveland, Ohio 44135

Acknowledgments

The authors would like to thank the NASA Revolutionary Vertical Lift Technology and Advanced Air Transport Technology projects for funding this work.

This report contains preliminary findings,
subject to revision as analysis proceeds.

This work was sponsored by the Advanced Air Vehicle Program
at the NASA Glenn Research Center

Trade names and trademarks are used in this report for identification
only. Their usage does not constitute an official endorsement,
either expressed or implied, by the National Aeronautics and
Space Administration.

Level of Review: This material has been technically reviewed by technical management.

Available from

NASA STI Program
Mail Stop 148
NASA Langley Research Center
Hampton, VA 23681-2199

National Technical Information Service
5285 Port Royal Road
Springfield, VA 22161
703-605-6000

This report is available in electronic form at <http://www.sti.nasa.gov/> and <http://ntrs.nasa.gov/>

An Investigation Into the Grain Structure of Impact Ice

Rebekah G. Douglass*
Pennsylvania State University
State College, Pennsylvania 16802

Andrew H. Work, Jr.
Ohio Aerospace Institute
Brook Park, Ohio 44142

Richard E. Kreeger
National Aeronautics and Space Administration
Glenn Research Center
Cleveland, Ohio 44135

Ernestina Schirmer
Purdue University
West Lafayette, Indiana 47907

Abstract

To design effective anti-icing and de-icing technology for aircraft, scientists and engineers must obtain a fundamental understanding of the microstructural characteristics of impact ice. This study investigates the effects of icing parameters, such as airspeed and liquid water content (LWC), on the impact ice microstructure near the interface to a metal substrate. Ice samples were accreted in the NASA Glenn Icing Research Tunnel (IRT) and tested in the NASA Revolutionary Icing Materials Evaluation Laboratory (RIMELab). A microtome was used to shave down the ice to a thickness of <1 mm for examination under a microscope. Samples were imaged at multiple magnifications by using bright-field imaging. The average grain size was determined for each sample in accordance with ASTM standard methods, and relationships between airspeed, LWC, and grain size were identified. It was observed that the average grain area in a given cross section was linearly related to the distance of the cross section from the metal surface. Finally, the effects of annealing and sublimation on the microstructure were also explored. The results show significant variation in the grain structure, suggesting a means by which icing conditions influence adhesion strength.

Nomenclature

G	ASTM grain size number
IRT	Icing Research Tunnel
LWC	Liquid Water Content [g/m^3]
MIST	Microscopic Ice Sizing Tool
MVD	Median Volumetric Diameter [μm]
R^2	Coefficient of Determination
RIMELab	Revolutionary Icing Materials Evaluation Laboratory

*Summer Intern in Lewis' Educational and Research Collaborative Internship Project (LeRCIP).

Introduction

Ice accretion on aircraft surfaces is a serious threat to flight safety. For decades, engineers have been combating the issue of aircraft icing through numerous means. Extensive testing has been performed in icing wind tunnels, which can accurately reproduce the temperatures, airspeeds, and cloud conditions encountered in atmospheric icing. The material properties of aircraft ice have largely been ignored in the literature but are of primary concern to many problems in the field of aircraft icing. Two of the main forces that affect icing physics include adhesive and cohesive forces. The term “cohesive” refers to the bonds between neighboring water molecules in the ice, while “adhesion” refers to the bonds between the ice water molecules and a substrate. If ice is to be removed from an aircraft structure, the adhesive bond between the ice and the aircraft must be overcome. Therefore, characterizing the adhesion properties of ice is critical to solving the icing problem. Despite this, there is little information available suggesting what property values should be used to simulate the failure of an adhesive bond. Literature data are available for annealed polycrystalline ice, but the data are dependent on the method of formation and the grain size (Refs. 1 and 2).

A study by Hidas et al. has shown that ice under stress, even at subfreezing temperatures, will change its crystal structure to minimize the free energy of the system (Ref. 7). In Hidas’ study, an ice sample was stressed at -7°C and the temperature was increased to -5°C . In less than an hour, some smaller grains had merged together and some larger grains had split to form smaller ones. After 24 hours, the grain structure was completely unrecognizable compared to its original state.

The Icing Research Tunnel (IRT) at the NASA Glenn Research Center has been used to test many different geometries—wings, tails, fuselages, probes, nacelles, rotor blades, and so on. Historically, most of these tests focused on the aerodynamics of icing, though some recent testing has focused on acquiring samples for the materials testing of impact ice with the primary purpose of obtaining adhesion data (Refs. 3 and 4). Variations in grain structure are expected to have significant effects on the material properties of ice, because among other effects, grain boundaries increase the plastic behavior of the ice (Refs. 1 and 2). To the knowledge of the authors, the grain structure of impact ice has only been quantified at low-impact velocities. Druetz et al. imaged the grain structure, or fabric, of ice at air velocities below 24 m/s, showing significant changes in adhesion strength and grain structure with velocity (Ref. 5). Capturing the variations in the fabric of ice at speeds relevant to aircraft icing is not only required for a better understanding of failure in an adhesive break but should be expected to provide a rationale for comparing material properties to icing parameters. The purpose of this study is to investigate how different icing parameters affect the grain structure of IRT ice samples, as observed under a microscope. Figure 1 shows two examples of glaze and mixed ice adhered to the test coupons utilized in this study.

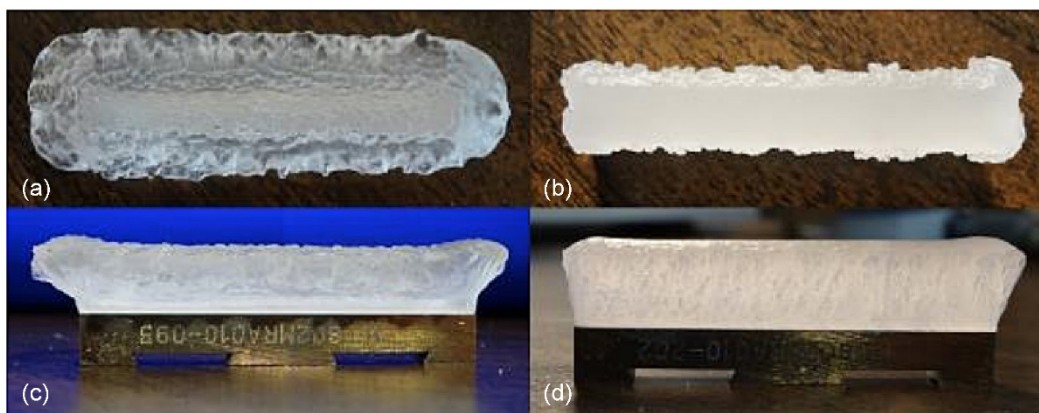


Figure 1.—Two IRT ice samples on stainless steel coupons. (a) Top view of glaze ice. (b) Top view of mixed ice. (c) Side view of glaze ice. (d) Side view of mixed ice.

The sample on the left in Figure 1(a) and (c) is qualitatively consistent with the glaze ice regime, which occurs in warmer temperatures and at higher LWCs. It is transparent due to the formation of a liquid film during the freezing process which tends to reduce the amount of air trapped in the ice. The sample on the right was accreted in mixed ice conditions (Figure 1(b) and (d)). The droplets froze more quickly upon impact, resulting in more trapped air and whiter ice as well as a geometry that better matches the form of the coupon surface. The differences in the way the ice forms in various icing regimes cause differences in the grain structure, which in turn affects the adhesion strength of the ice. This is in general agreement with the literature; authors have reported different adhesion strengths with regard to temperature and icing conditions (Ref. 6).

Methodology

Slicing

The samples were obtained from the IRT, as in a previous study (Ref. 3). After the ice samples were accreted in the IRT, the iced metal coupons were carefully removed from their mounts and placed in labeled bags. All the bags were then transported in a temperature-controlled cooler to a separate walk-in freezer, which was maintained at the same temperature as the IRT test conditions. Inside the freezer, the metal coupons were placed in a vise and the ice was sliced down by using a microtome, as shown in Figure 2 and Figure 3. The samples used for grain size analysis in the July 2018 IRT test were sliced and

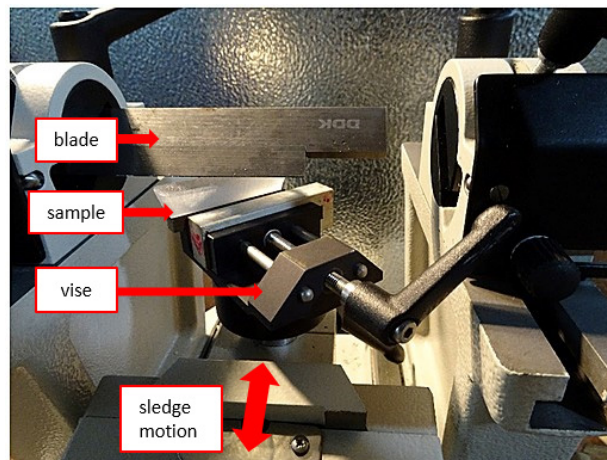


Figure 2.—Ice sample being sliced in the microtome.

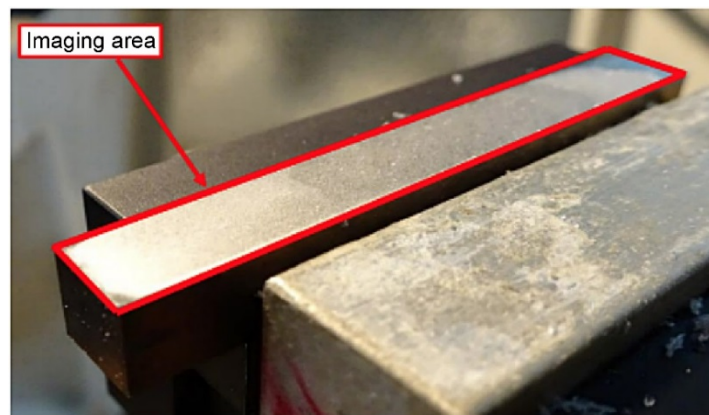


Figure 3.—Sample AQ324 (0.198 mm thick).

imaged within 1 hour of being removed from the IRT (unless otherwise stated) to minimize uncertainty due to transient effects. The samples were maintained within ± 2 °C throughout the transportation and cutting process, and the data was collected within a short time. Improved testing would be needed to quantify shorter term changes in the ice.

As shown in Figure 2, ice samples were cut at an angle to reduce loading on the sample, maintaining the interface as close to parallel to the sled travel as possible. The microtome’s precise ratcheting mechanism permitted slices as thick as 40 microns and as thin as 1 micron. The samples could be cut very thin without cracking—in the case of Sample AQ324 in Figure 3, as thin as 0.2 mm.

Visualization

After the ice was sliced, it was placed under a microscope to be examined and photographed. To extract meaningful quantitative data from the microscope photographs, scale factors were established to perform physical measurements with the images. A glass calibration slide was photographed at four magnifications to obtain the conversion factors listed in Table 1.

The microscope allowed the ice to be viewed by using either reflected or transmitted light. Using transmitted light required the ice to be removed from the metal substrate and placed on a glass slide for viewing. To minimize damaging or altering the ice microstructure, the ice in this study was not removed from the original metal coupons. Therefore, since the coupons were opaque, only reflected light microscopy was used. Although this method helped preserve the original ice microstructure, background noise was introduced by imperfections in the metal surface, which would have been avoided with clear glass slides. Figure 4 shows sample photographs taken after the IRT test.

TABLE 1.—CONVERSION FACTORS BETWEEN PIXELS AND MILLIMETER FOR DIFFERENT OBJECTIVE LENSES

Magnification	×1.25	×5	×10	×20
Scale factor (pixel/mm)	195	772	1,544	3,138

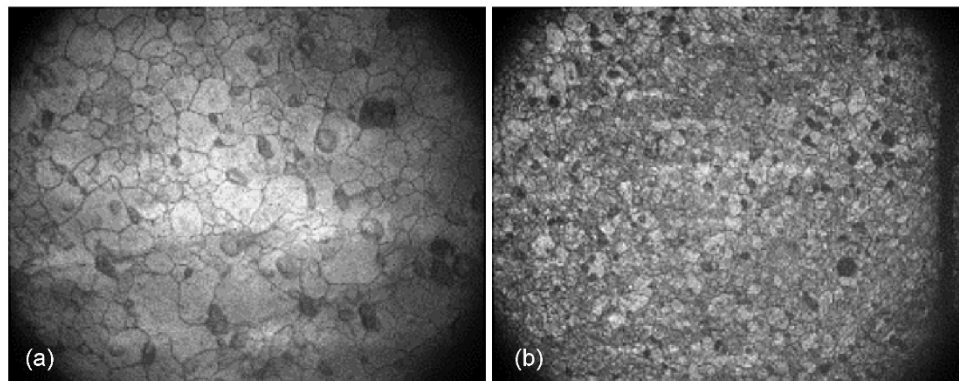


Figure 4.—Samples under magnification. (a) Sample AK39 at ×10 magnification. (b) Sample AQ342 at ×5 magnification.

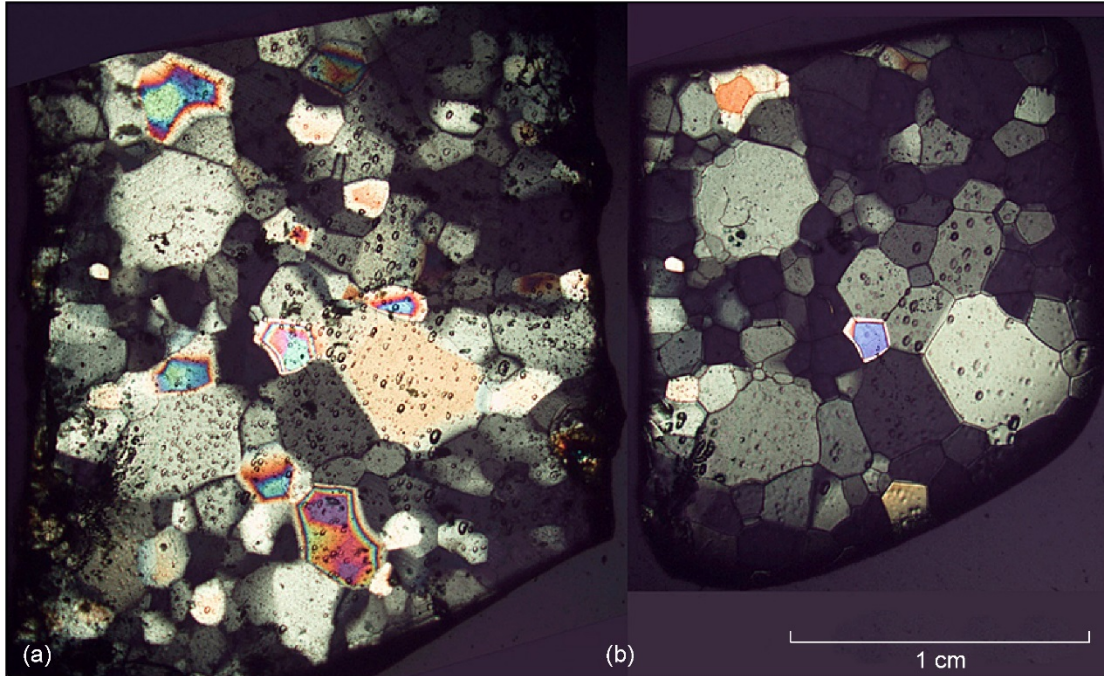


Figure 5.—Sample E15. (a) Image taken immediately after cut. (b) Image taken one day later.

A white light source was used to produce bright field illumination for all images in this study. However, in future studies, it may be advantageous to use polarized light. Polarized light microscopy uses filters to shine plane-polarized light into the sample. The light refracts in the anisotropic crystal structure of the ice and yields a colorful view of the structure and orientation of the grains. Cross-polarized images were taken, however, grain boundaries were obscured due to the presence of very small grains near the interface. An example of ice viewed with polarized light can be seen in Figure 5.

Sublimation

In icing research, sublimation and/or deposition on ice samples may be problematic. However, when the goal is to visualize the crystal structure, these mechanisms can be very useful. Nelson explains that edges and grain boundaries in the crystal structure are the primary sites for mass removal by sublimation or mass addition by deposition (frost) (Ref. 8). For an example, see Figure 5.

Grain Size Analysis

To obtain an average ice grain size for each sample, three ASTM standard methods were applied (Ref. 9). The first was Heyn's linear intercept method, which involves counting the number of grains intercepted by a grid of straight test lines of known length. Grains at the ends of a test line are also counted as half-grains. The total number of intercepted grains over the total length of the lines determines the ASTM grain size.

Hilliard's circular intercept method works much the same way and uses the circumference of a circular test region. The circle eliminated the possibility of error being introduced due to the ends of straight test lines ending midgrain, and it also eliminates any directional bias regarding grain growth (such as grains elongated more so in the x-direction than the y-direction), making it useful for materials with nonequiaxed grains.

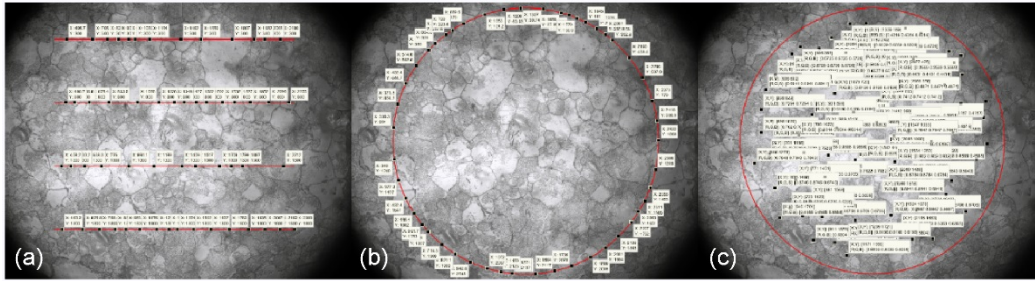


Figure 6.—Sample AM136 subjected to different methods. (a) Linear intercept method. (b) Circular intercept method. (c) Circular planimetric method.

The third method applied to the microscope images was the planimetric, or Jefferies, procedure. Jefferies' method involves counting the number of grains fully enclosed by a test circle and counts intercepts as half-grains. The number of grains counted and the area of the circle determine the average grain size. The necessary equations to calculate the average grain diameter for each of the three methods are outlined in the ASTM guidelines.

As the number of counted grains increases, so does the accuracy of the average grain size. Heyn and Jefferies both recommend a minimum sample size of 50 grains. For the Hilliard method, a minimum of 35 intercepts per test circle is advised. The ASTM guidelines attribute a majority of the uncertainty in these methods to the fact that grain sizes can vary widely from one field of view to another. To achieve a relative accuracy of 10%, at least 700 grains total must be counted using the planimetric method, and at least 400 grains with the intercept method (Ref. 9). (In this sense, the relative accuracy of intercept methods is higher than the planimetric method for the same number of counts.) Obtaining sample sizes of that magnitude were unrealistic in the current study because the coupons only had an area of 2×0.25 in.

In the current study, typically only three to five fields of view were examined near the center of each coupon for grain size analysis. The accuracy of the analysis increases with the number of grains counted, so photos would be taken across the entire coupon area to maximize the reliability of the results. For analysis purposes, the $\times 1.25$ photographs were not useful because individual grains were too small to resolve. On the $\times 20$ lens, the grains appeared so large that only a few grains would appear in the field of view—not a large enough sample size. Therefore, the $\times 10$ and $\times 5$ provided more suitable images. The $\times 10$ allowed grain boundaries to be seen very clearly, and the $\times 5$ was useful for getting multiple sampling areas out of a single photo.

A MATLAB[®] (MathWorks[®]) script, called the Microscopic Ice Sizing Tool (MIST), was developed to automate the grain size calculations. The user selects the desired microscope image and then selects a grain sizing method to use. Within a generated MATLAB[®] figure, the user selects the intercepts in the case of the Heyn and Hilliard method or the interior grains and intercepts in the Jefferies method. Then, the average grain diameter is calculated by using the microscope image scale factors and formulas from the ASTM guidelines. Sample images from the MIST script are shown in Figure 6.

Microscope Images and Data from July 2018 IRT Test

Test Conditions

Table 2 shows the test matrix for the July 2018 IRT test. Two different airspeeds were tested, and for each airspeed, an LWC sweep was performed. The use of a single total temperature allowed samples to be stored at the same temperature with little risk of cracking from thermal expansion.

TABLE 2.—TEST MATRIX FOR THE JULY 2018 IRT TEST

Run label	MVD (μm)	Total temp. (°C)	Airspeed (kn)	Static temp. (°C)	Nozzle type	LWC (g/m ³)
AK	20	-10	150	-12.9	Mod 1	0.4
AL	20	-10	150	-12.9	Mod 1	0.8
AM	20	-10	150	-12.9	Standard	1.2
AN	20	-10	150	-12.9	Standard	1.6
AO	20	-10	150	-12.9	Mod 1	0.4
AP	20	-10	200	-15.2	Mod 1	0.3
AQ	20	-10	200	-15.2	Mod 1	0.65
AR	20	-10	200	-15.2	Standard	1

The primary purpose of the IRT run was to obtain adhesion samples, however, samples from each run were sliced down and observed under the microscope for this study. For the first three runs, photographs were taken at $\times 10$ magnification but were taken at $\times 5$ for the last five runs.

Grain Size as a Function of LWC and Airspeed

Both the circular intercept and circular planimetric methods were applied to the same photographs for comparison. Table 3 shows the thickness values to which the sample from each run was cut. It also lists the mean grain diameter obtained from photographs of the center of each coupon.

The mean grain diameters for the circular planimetric and circular intercept method varied by less than 15% for all runs, except for AQ342. To investigate the large error on the photo from AQ342, two additional circular test regions on the same photo were selected and analyzed. As is shown in Table 4, when the test areas were averaged, the difference between the methods fell to 2%. This suggests that the difference between the two techniques was due to a variation in the grain structure over the averaging regions—suggesting that the area used for measurement was not sufficient to capture the spatial variation in this sample.

The average grain area was plotted as a function of analysis method, airspeed, and LWC in Figure 7. Since the ice growth rate varies with LWC, it was hypothesized that the differing thermodynamics of formation would cause a variation in grain structure. The linear trendlines fit to the data in Figure 7 exhibit a positive trend between LWC and grain size for a constant velocity. However, a high degree of scatter exists in the data set, especially for the 150-kt case. This may suggest that grain size is actually independent of LWC at that speed. A regression analysis performed on the data set determined that the 150-kn trendline was not statistically significant with a p-value of approximately 0.7. The 200-kn trendlines were steeper than the 150-kn trendlines; it was unclear why this was the case. A regression analysis could not be performed on the 200-kt case because there were too few points. It is clear that more data is required to draw conclusions about the relationship between LWC and grain size.

The scatter in the data was likely due to the fact that only one location was photographed on each coupon, and only one coupon per IRT run. This decision was made due to time constraints, but in future experiments, multiple samples should be sliced from each IRT run, and the grain size should be averaged over multiple locations on the coupon. Additionally, the images were taken at varying heights since the ice layer thickness could not be measured with perfect precision. Human error while clamping the coupon in the microtome vise or adjusting the microtome blade was a potential source of error since any small misalignment would cause the ice to not be sliced perfectly evenly across the coupon. The ice thickness values reported in this paper were measured using a digital micrometer with a resolution of 0.001 mm; however, it should be noted that the ice thickness uncertainty is larger than that. Since the ice was sliced

TABLE 3.—MEAN GRAIN DIAMETER RESULTS FOR A SINGLE COUPON PER TEST RUN

Run label	Thickness after cut (mm)	Magnification of photo	Airspeed (kn)	LWC (g/m ³)	Mean grain diam.: Jeffries' method (mm)	Mean grain diam.: Hilliard's method (mm)	Difference (%)
AK039	0.444	×10	150	0.4	0.087	0.085	2.1
AL092	0.383	×10		0.8	0.095	0.102	7.9
AM136	0.341	×10		1.2	0.094	0.082	14.1
AN186	0.351	×5		1.6	0.098	0.108	11.0
AO243	0.509	×5		0.4	0.102	0.102	0.3
AP290	0.385	×5	200	0.3	0.073	0.068	6.1
AQ342	0.539	×5		0.65	0.076	0.093	23.1
AR356	0.591	×5		1	0.088	0.100	13.3

TABLE 4.—RESULTS OF ADDITIONAL ANALYSIS ON SAMPLE AQ342

Sample:	Mag: ×5	Original location	Mean grain diameter:	Mean grain diameter:	% Difference
			Jeffries' method (mm)	Hilliard's method (mm)	
AQ342	×5	Original location	0.076	0.093	2.36
		Second location	0.084	0.077	
		Third location	0.085	0.069	
		Average	0.081	0.080	

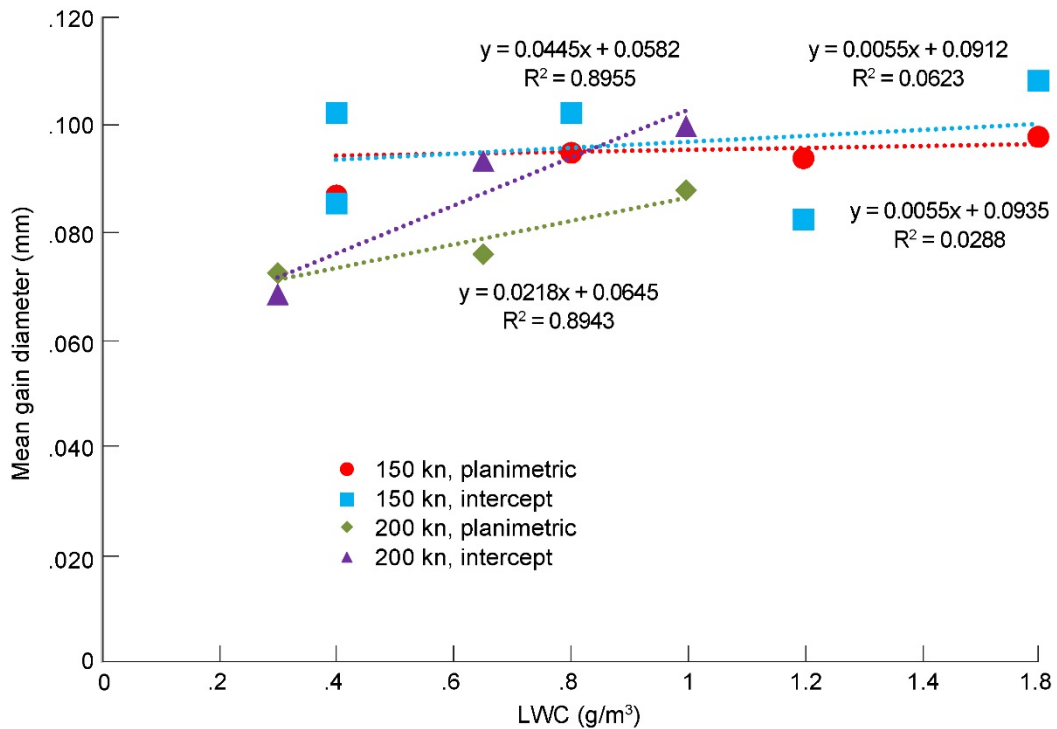


Figure 7.—Graph of data from Table 3—mean grain diameter as a function of airspeed and LWC.

so thin, even light clamping with the micrometer cracked the ice. It was therefore decided that the ice thickness should be measured on one edge of the coupon only, so as to avoid ruining the ice specimen for microscope photos. Thus, it was unknown to what degree the sliced ice thickness varied over the length of the coupon, or to what degree ice cracking affected the thickness values. In future studies, it is recommended that the use of a micrometer be avoided, and that sideways microscope photos be used instead to approximate the thickness.

It is also worth noting the discrepancy between the grain sizes of runs AK and AO, which had identical run parameters (150 kn, LWC = 0.4) but different grain sizes. The likely reason for this discrepancy is that during the IRT test, a “false start” was recorded during runs AK and AM—in other words, the cloud spray was turned on prematurely. If one of the two LWC = 0.4 points should be trusted, it would be the second one (run AO). This illustrates another potential source of error: the ice accretion process inside the IRT. Impact icing is a dynamic process, so the cloud experienced by any given coupon varies with time. According to Steen et al. (Ref. 10), the local LWC in a majority of the test section area is within 10% of the average LWC. Additionally, the MVD deviates less than 10% from the calibration curves. The 10% variation of cloud parameters leaves room for potentially significant and poorly understood differences in the microstructure of the ice. Coupons located in the center of the test section could have different grain sizes than coupons closer to the tunnel walls, solely due to time-varying MVD and LWC. Especially for the initial layers of grains at the coupon interface, the first few seconds of cloud spray are crucial.

Grain Size as a Function of Ice Thickness

An extra sample from run AO was sliced sideways, so that the ice structure normal to the interface could be observed. Figure 8 shows a photo taken of the ice crystals as they grew away from the interface.

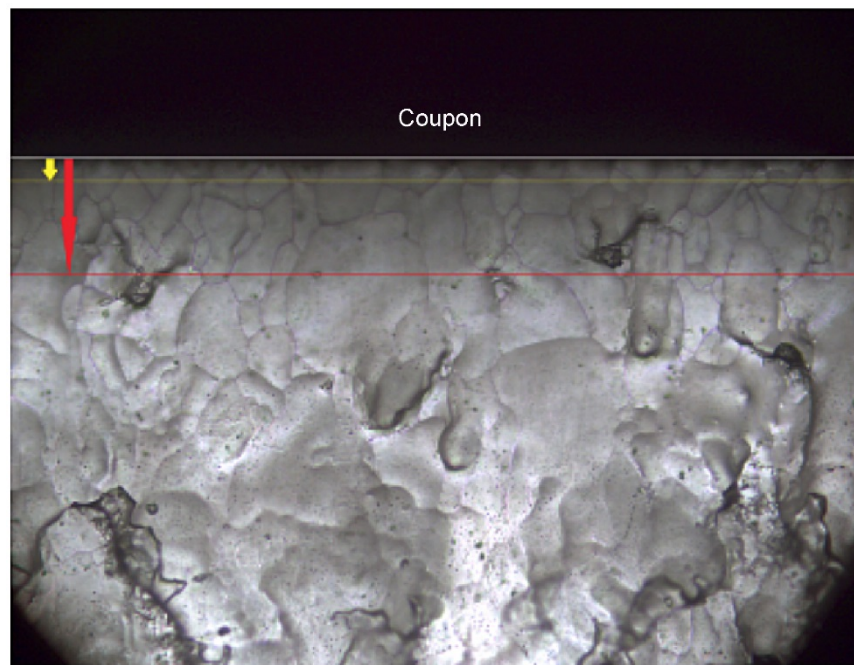


Figure 8.—Side view of sample AO202. Yellow line is 0.10 mm from coupon surface. Red line is 0.50 mm from coupon surface.

The grains at the surface were smaller than the grains away from the interface, and a very thin layer of grains existed at the interface that was difficult to image. This was likely caused by changing thermodynamics; the first layer of drops freezes quickly on the cold metal, but as more ice accretes, the previous layers of ice insulate the new layers. It was determined that the first layer of crystals large enough to be characterized on sample AO202 was only about 0.1 mm thick. Most samples were cut as close to this depth as possible to capture the size of these grains.

To quantify how the grain size varied throughout the ice thickness, sample AQ324 was sectioned at multiple depths to check the variation in grain size with thickness. The microscope stage was adapted so the coupon could be placed in two precise locations after every cut: the coupon center and the coupon edge. A schematic is shown in Figure 9.

Figure 10(a) shows the grain structure at level 1 at the coupon edge; only ten grains are visible at $\times 5$. Cut levels 2-4 looked like Figure 10(b); few grain boundaries were visible, if any at all, at the coupon center and edge. It is not clear why this occurred, but those three photographs were unusable for analysis. At cut levels 5-7, the grains were clear enough to be counted, though at level 7, delamination of the ice and the visible metal surface made analysis difficult. The delamination is clearly visible in photographs taken at the metal interface, shown in Figure 11.

Near the center of the coupon shown in Figure 11, the ice still seems firmly attached to the coupon with only a few bubbles. Moving toward the edge, smaller features become more pronounced. This may have been due to a smaller layer of grains, delamination of the ice, or both. This difference is actually visible as discoloration on the edge of the coupon and can be faintly seen in Figure 3.

Table 5 shows the results of grain analysis at levels 1, 5, 6, and 7. These data are plotted in Figure 12. It was expected from previous observations that there would be a relationship between grain size and the distance from the metal interface. A linear regression provided a good fit of the data with $R^2 > 0.98$, and is in good qualitative agreement with observations.

Finally, the grain size from samples AL092 and AL093 was compared (see Figure 13, Table 6), which should have near-identical ice since they were positioned side-by-side during the IRT test. Sample AL092 had been cut to 0.4 mm thickness; sample AL093 cleanly delaminated from the coupon while it was being cut, so it was flipped over and observed directly where the grains had been touching the metal. Both analysis methods showed that the grains in AL093 (at the interface) were 0.004 mm^2 smaller than the grains at a thickness of 0.4 mm on AL092, which is a 40% reduction in size.

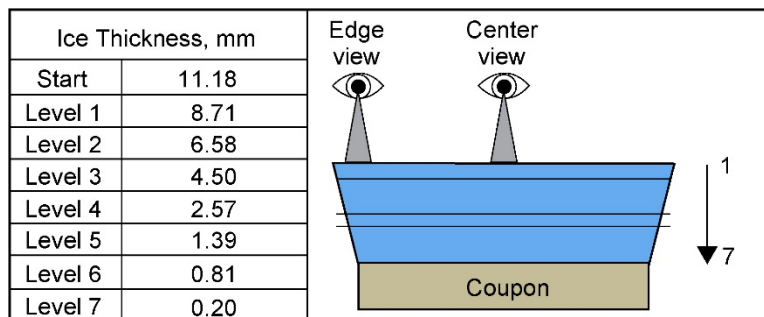


Figure 9.—Schematic of “cut down” analysis on sample AQ324.

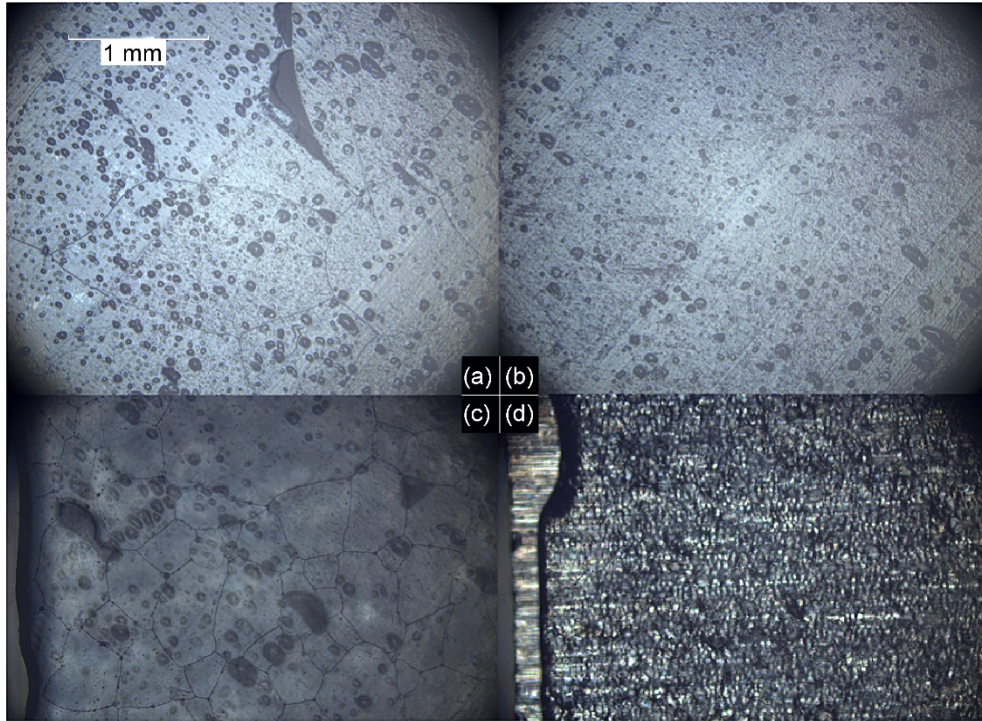


Figure 10.—Sample AQ324 edge location cut levels. (a) Cut level 1. (b) Cut level 3. (c) Cut level 6. (d) Cut level 7.



Figure 11.—Photographs of lengthwise microstructure at metal interface.

TABLE 5.—RESULTS OF “CUT DOWN” ANALYSIS

Cut level	Ice thickness (mm)	Average grain area at edge (mm ²)	Average grain area at middle (mm ²)	Analysis type	
				Hilliard	Circular intercept
1	8.712	1.508	0.762	Hilliard	Circular intercept
5	1.392	0.277	0.165	Hilliard	Circular intercept
6	0.805	0.127	0.145	Heyn	Linear intercept
7	0.198	0.035	0.080	Heyn	Linear intercept

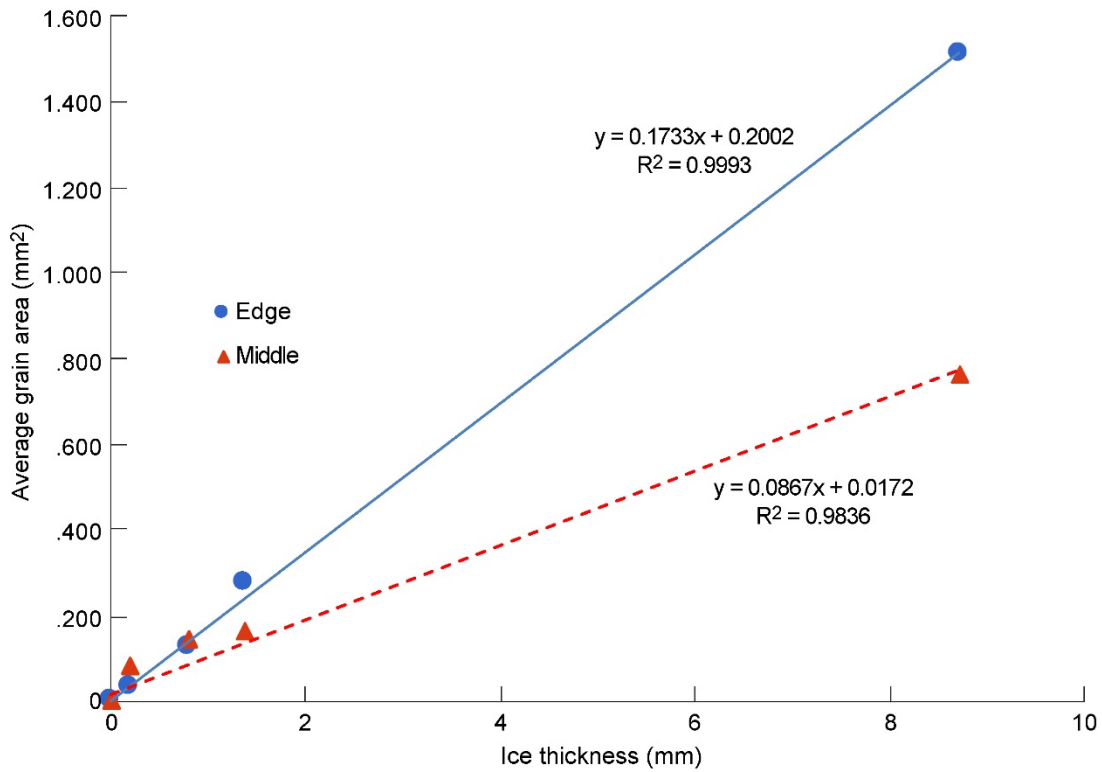


Figure 12.—Plot of Table 5 data—average grain area as function of ice thickness on sample AQ342.

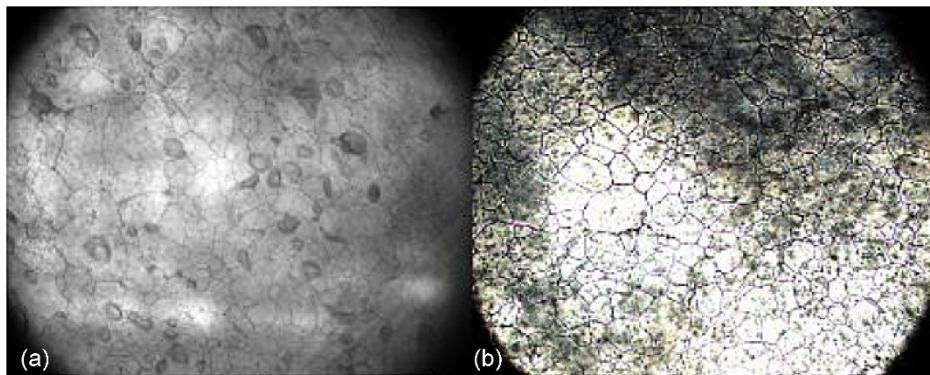


Figure 13.—Photographs of grain structure at coupon center, $\times 10$ magnification. (a) AL092. (b) AL093.

TABLE 6.—COMPARISON OF MEAN GRAIN AREA FROM SIMILAR ICE AT DIFFERENT THICKNESSES

Sample	Distance from coupon surface (mm)	Mean grain area: linear intercept (mm ²)	Mean grain area: circular intercept (mm ²)
AL092	0.38	0.0117	0.0105
AL093	0.00	0.0075	0.0067

Recrystallization

It was hypothesized that the sample interface might recrystallize during storage, and that the corners of the coupon would be high-stress regions suitable to capture such recrystallization. To investigate this theory, several samples were investigated in more detail at the corners and one over a lapse in time. For the first sample, the average grain size at the corners of sample AQ342 was compared to the average grain size at the center of the coupon. The results are shown in Table 7.

The grains in the center of the coupon were shown to be 26% smaller than at the corners. This analysis was performed on the same night as the IRT test. Eighteen days after the IRT test, the corners of sample AQ324 were photographed a second time to investigate possible recrystallization. Many of the grain edges were blurred and the ice near the coupon edges sublimated away. Unfortunately, images suitable for analysis were not taken before the sample was destroyed, but qualitative observation of the photographs shows that the grain sizes appear to be more uniform 18 days after the test. One common set of grains were identified and highlighted in red in Figure 14. Using this as a reference point, many of the same grains can be identified between the two samples, providing weak evidence for recrystallization.

The sample AQ342 was marked with a notch to help serve as a reference point, however, the sample sublimated enough that the notch was removed. While the grain boundaries may have moved or blurred, this may have been due to a thinning of the ice. Different imaging techniques are likely required to improve image quality near the interface since the size of the grains is small compared to the layer thickness. Given prior results showing a variation in the adhesion strength with annealing time (Ref. 3), further study is warranted.

TABLE 7.—CORNER VERSUS CENTER GRAINS COMPARISON ON SAMPLE AQ342
[Examined on test day, July, 23, 2018, at 0.54 mm thickness.]

Location	G ^a	Average grain area (mm ²)	
Corner 1	3.453	0.01178	0.00997
Corner 2	3.766	0.00949	
Corner 3	3.819	0.00914	
Corner 4	3.772	0.00945	
Middle	4.131	0.00736	-----

^aASTM grain size number.

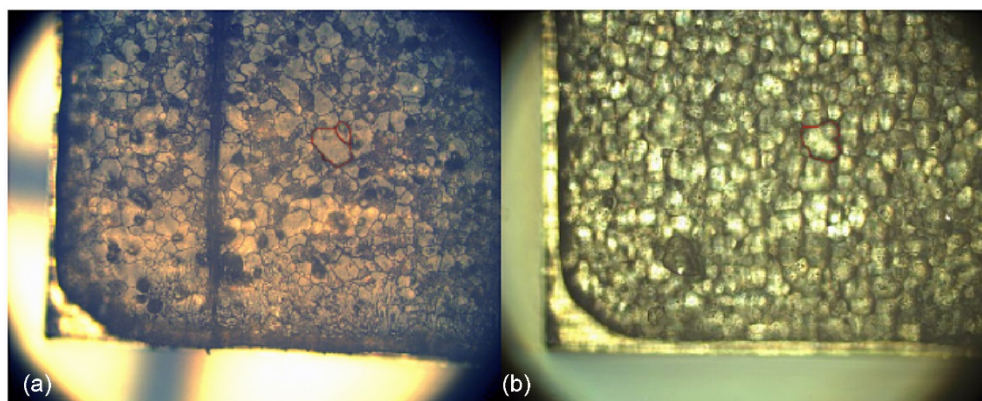


Figure 14.—AQ342 corner photographs with reference grains outlined in red. (a) July 12, 2018. (b) July 30, 2018.

Conclusions

The series of data examined demonstrates the variation of the grain structure with respect to several key variables, including velocity and cloud liquid water content. It has been shown that the grain structure of the ice varies spatially over our samples to some degree. More importantly, the fabric exhibited a linear relationship with distance to the interface, though this may not hold at distances further from the interface. More data is required to draw conclusions about the relationship between grain size and LWC. The 200 kt case did not contain enough points to run a regression analysis, and the 150 kt case exhibited such a high degree of scatter that the trend was not statistically significant. The results suggest that the material properties of ice, especially those characterizing fracture, should be expected to vary close to the interface compared to the bulk of the ice. This suggests that future studies should investigate the variation of the fabric as varying with distance from the interface more extensively. More data needs to be gathered to understand the full implications for adhesive studies. Recrystallization was not conclusively observed in a sample sitting for over two weeks. Further study is also needed to investigate the effects of the droplet mean volumetric diameter (MVD) and the air temperature on the grain structure.

References

1. Schulson, E.M., Duval, P., 2009. Creep and Fracture of Ice. Cambridge University Press, New York.
2. Hobbs, P.V., 1974. Ice Physics. Clarendon Press, England.
3. Work Jr., A.H., 2018. The measurement of the adhesion of glaze ice. University of Louisville Electronic Theses and Dissertations, Paper 2987. <https://doi.org/10.18297/etd/2987>
4. Work Jr., A.H., et al., 2018. An experimental study of the adhesion strength of impact ice, in 2018 Atmospheric and Space Environments Conference, AIAA 2018–3341. <https://doi.org/10.2514/6.2018-3341>
5. Druetz, J., et al., 1979. The adhesion of glaze and rime on aluminum electrical conductors. T. Can. Soc. Mech. Eng. 5, 215–220.
6. Work, A., Lian, Y., 2018. A critical review of the measurement of ice adhesion to solid substrates. Prog. Aerosp. Sci. 98, 1–26.
7. Hidas, K., et al., 2017. Microstructural evolution during thermal annealing of ice-Ih. J. Struct. Geol. 99, 31–44.
8. Nelson, J., 1998. Sublimation of ice crystals. J. Atmospheric Sci. 55, 910–919.
9. American Society for Testing and Materials, 2012. Standard Test Method for Determining Average Grain Size. ASTM–E112–13, West Conshohocken, PA, pp. 1–28.
10. Steen, L., et al., 2015. NASA Glenn Icing Research Tunnel: 2014 and 2015 Cloud Calibration Procedures and Results. NASA/TM—2015-218758.

